7-2017

Atomistic Quantum Transport Simulation of Multilayer Phosphorene Nanoribbon Field Effect Transistors

Hojjatollah Sarvari
University of Kentucky

Chaoyuan Liu
Eastern Kentucky University

Amir Hossein Ghayour
Shiraz University

Parham Shenavar
Shiraz University

Zhi Chen
University of Kentucky

See next page for additional authors

Recommended Citation

Hojjatollah Sarvari, Chaoyuan Liu, Amir Hossein Ghayour, Parham Shenavar, Zhi Chen and Rahim Ghayour, Atomistic Quantum Transport Simulation of Multilayer Phosphorene Nanoribbon Field Effect Transistors, Physica E: Low-dimensional Systems and Nanostructures, http://dx.doi.org/10.1016/j.physe.2017.04.015

Authors
Hojjatollah Sarvari, Chaoyuan Liu, Amir Hossein Ghayour, Parham Shenavar, Zhi Chen, and Rahim Ghayour

Atomistic Quantum Transport Simulation of Multilayer Phosphorene Nanoribbon Field Effect Transistors

Hojjatollah Sarvari, Chaoyuan Liu, Amir Hossein Ghayour, Parham Shenavar, Zhi Chen, Rahim Ghayour

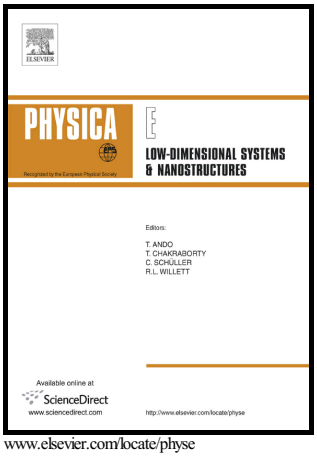

www.elsevier.com/locate/physe

PII: S1386-9477(17)30006-1
DOI: http://dx.doi.org/10.1016/j.physe.2017.04.015
Reference: PHYSE12788

To appear in: *Physica E: Low-dimensional Systems and Nanostructures*

Received date: 3 January 2017
Revised date: 15 April 2017
Accepted date: 20 April 2017

Cite this article as: Hojjatollah Sarvari, Chaoyuan Liu, Amir Hossein Ghayour Parham Shenavar, Zhi Chen and Rahim Ghayour, Atomistic Quantum Transpor Simulation of Multilayer Phosphorene Nanoribbon Field Effect Transistors *Physica E: Low-dimensional Systems and Nanostructures* http://dx.doi.org/10.1016/j.physe.2017.04.015

Atomistic Quantum Transport Simulation of Multilayer Phosphorene Nanoribbon Field Effect Transistors

Hojjatollah Sarvari[1], Chaoyuan Liu[2], Amir Hossein Ghayour[3], Parham Shenavar[4], Zhi Chen[1], and Rahim Ghayour[4*]

[1]*Department of Electrical & Computer Engineering and Center for Nanoscale Science & Engineering, University of Kentucky, Lexington, Kentucky 40506, USA*

[2]*Department of Mathematics and Statistics, Eastern Kentucky University, Richmond, Kentucky 40475, USA*

[3]*Department of Chemical Engineering, Shiraz University, Shiraz, Fars 71866, Iran*

[4]*Department of Electronic & Communication Engineering, Shiraz University, Shiraz, Fars 71866, Iran*

[*] *Corresponding author: e-mail: rghayour@shirazu.ac.ir*

Tel: +98-917-7055393 Fax: +98-711-6133053

Abstract— **Few-layer black phosphorus is a semiconductor material, where its allotrope is called phosphorene; a new two-dimensional material which is discovered in 2014. In this paper, first we use the tight-binding method to implement a matrix representation for single-layer and multilayer structures of phosphorene nanoribbon (PNR) to define the Hamiltonian of the system. Second, we investigate the band structure and the band gap of multilayer PNRs. The band gap of armchair PNRs with 16 atoms across the width of PNR for single-layer, bilayer, and three-layer structures are obtained as 1.899, 1.224, and 0.937 eV, respectively. Third, we use the atomistic description of structure to simulate the performance characteristics of single and multilayer PNR field effect transistors (PNRFETs) by employing the non-equilibrium Green's function (NEGF) formalism. Based on the properties of the material and device structures, I_d-V_{gs}, I_d-V_{ds} characteristics, energy band diagram in the channel, and I_{ON}/I_{OFF} are analyzed. The ON to OFF current ratio for single-layer, bilayer, and three-layer PNRFETs are increasing when the channel length increases from 5nm to 15nm. The current ratio for single-layer increases from 1277 for L_{ch}=5nm to 216.7×10^6 for L_{ch}=15nm. The I_{ON}/I_{OFF} in single-layer PNRFET is higher in comparison with those values in bilayer and three-layer PNRFETs due to very small off-current in the single-layer PNRFET which in turn resulted from its larger band gap. The results show that the performance of PNRFET changes significantly depending on the number of phosphorene layers and the length of the channel of device.**

Keywords: multilayer phosphorene nanoribbon; tight-binding; PNRFETs; Green's function;

1. Introduction

Since 2004, a number of two-dimensional (2D) materials have been discovered such as Graphene, Molybdenum Disulphide (MoS_2), Arsenene, and Black Phosphorus (BP). Graphene as a 2D sheet of carbon atoms with thickness of only one atom was the first 2D material discovered in 2004, which has attracted a great attention in the semiconductor industry, particularly in electronic devices, interconnects, and energy storage [1-5]. The main issue for graphene is its lack of energy bandgap which, limits its application as a material for electronic devices such as field effect transistors (FETs), because graphene devices cannot be turned OFF completely. BP in its layered form which is named "*phosphorene*", is a 2D semiconductor material discovered in 2014. It shows interesting electronic, semiconducting and optical properties [6-9]. Phosphorene, like graphene, can be produced as thin as one single atomic layer. In fact, BP bulk crystal is composed of many individual layers stacked up over together by van der Waals force; however, unlike graphene layers which are perfectly flat, phosphorene layers form a puckered surface due to the sp^3 hybridization [10].

The phosphorene nanoribbons (PNRs) can be obtained by cutting a single-layer phosphorene along its armchair or zigzag directions in the same way as the graphene nanoribbon (GNR) is produced. Therefore, the armchair PNRs (A-PNRs) or zigzag PNRs (Z-PNRs) can be identified by the number of dimer lines or the zigzag chains across the ribbon width, respectively [8]. Both A-PNRs and Z-PNRs have positive and much smaller formation energies compared to the GNRs, which means that the experimental synthesis of PNRs is fully accessible [11]. According to the research history of the previous 2D materials such as graphene and MoS_2, the theoretical and simulation research studies of PNRs are necessary for future experimental works. Edge disorder is a problem in GNRs and therefore, patterning will be relatively difficult due to significant changes in the band gap of GNRs by different numbers of atoms across its widths, especially in narrower GNRs [12]. However, it should be mentioned that recently a group of scientists found a way to yield atomically precise zigzag graphene nanoribbon edges [13]. The band gap of GNR changes significantly by changing the number of carbon atoms within the width of ribbon, however by changing the

number of phosphorous atoms within the width of the ribbon, the variation of band gap of PNR becomes very small and thus negligible. This makes the fabrication of PNRs more convenient [14-19].

Theoretical and experimental studies have been carried out on few-layer phosphorene transistors. Various articles on phosphorene have been published since Liu et al. discovered phosphorene as a new 2D semiconductor material in 2014 [7, 9, 20-23]. For example, doped contact multilayer (ML) phosphorene FETs are simulated by self-consistently solving the 2D Poisson's equation and Schrodinger's equation based on NEGF in mode space [23]. FETs which use phosphorene as the channel material with a thickness of a few nanometers (meaning a few layers of phosphorene) were fabricated [7, 20, 24, 25]; however, in most of these experimental research articles, Schottky barriers junctions are used as the source and drain contacts [7, 9, 20, 26]. Multilayer Schottky barrier phosphorene FETs are also simulated using NEGF and 2D Poisson's equation based on atomistic structure of the channel calculated from the k.p model with a band gap of 1.52 eV. The results show ambipolar behavior with a high leakage current in multilayers that can be reduced by several orders of magnitude in single- and bilayer phosphorene FETs [22]. The effect of layer stacking orders (similar to layer stacking of AA, AB, and AC in GNR) of bilayer black phosphorene on the device properties of MOSFETs create possible chances to immunize FETs against short channel effects [27]. Single-layer BP FETs outperform both MoS_2 and SiFETs, either n- or p-type devices, due to higher carrier velocity in the armchair direction [21]. Wan et al. simulated single-layer phosphorene tunneling FETs (TFETs) via a self-consistent atomistic quantum transport based on the recursive scattering matrix approach using the density functional theory (DFT), where the band structure calculation resulted in a 0.93 eV band gap [22]. The proposed TFET exhibits a subthreshold slope (SS) below 60 mV/dec. Their results show that the on-current, I_{ON}, is dependent on the transport direction due to highly anisotropic band structure of phosphorene [19]. It also shows I_{ON} three orders of magnitude larger at the same I_{ON} /I_{OFF} ratio compared to that of the single-layer $MoTe_2$ TFETs, where it suggests superiority of phosphorene for TFETs application [19].

Cao et al. demonstrated that single-layer phosphorene FETs are promising candidates for the International Technology Roadmap for Semiconductors (ITRS) for the 2024 horizon [23]. Authors used the old version of tight-binding parameters which resulted in a band gap energy of 1.6 eV [23]. Another way to define the Hamiltonian of the system is to use the k.p method [22, 23]. However, the k.p method is based on the effective mass approximation whose applicability is not well justified for BP and its Hamiltonian is not well suited for studying real space problems even in the low-energy range [28]. The tight-binding method [29] shows fairly accurate energy band structures for phosphorene materials compared to the results based on the k.p method. More importantly, the results from tight-binding method are comparable to the first-principle calculations based on the DFT approach, especially in the low energy regime. Thus, we use the new tight-binding parameters to determine the Hamiltonian of the system. The parameters of tight-binding model for BP with an arbitrary number of layers were derived from partially self-consistent GW0 approach and presented for the first time by Rudenko et al [28, 30].

To the best of our knowledge, there is no quantum transport simulation study on SL- and ML-PNRFETs that uses NEGF with new TB parameters in literature so far. Our paper overcomes this limitation by utilizing new tight-binding parameters to form a matrix representation for single-layer and multilayer PNR structures. The defined matrix representation is used in the quantum transport simulation of PNRFETs using the NEGF formalism and 2D Poisson's equation [31, 32]. We explore the A-PNRs because of anisotropic properties of band structure of phosphorene, which enable electrons to travel faster in the direction of the armchair. This suggests that the armchair direction in the 2D plane has the highest carrier mobility [17, 22].

2. Theoretical Method

In this section, we have presented realistic matrix representations of SL- and ML-PNRs. The modified tight-binding parameters are introduced and used to simulate the PNR FETs based on the non-equilibrium Green's function formalism. Fig. 1 shows the view, the hopping parameter and the ball-stick model of the atomic structure of multilayer black phosphorus. In order to implement the tight-binding method, we use the atomic structure of (SL) layer phosphorene as shown in Fig. 1 (c). We supply all the model definitions in order to construct the Hamiltonian of the system for both the band structure calculation and the device simulation. The unit cell of phosphorene is composed of four atoms named as P_1-P_4 as shown in Fig. 1(c). The basis vectors are a_1 and a_2 along the armchair and zigzag directions, respectively. The length of a_1 and a_2 are 4.43 A° and 3.27 A°, respectively [6]. In order to have a direct bandgap material, we add hydrogen atoms to passivate the edge phosphorus atoms as shown in Fig. 1 (c) [8].

In our previous paper, we used the simple five-element TB parameters to investigate the electronic properties of phosphorene nanoribbons under the external modulated electric fields [16]. However, in this work, we apply the new ten-element TB parameters to determine the Hamiltonian of an A-PNR-FET for implementation of the quantum

transport method in the NEGF formalism. The proposed matrix representation of phosphorene structures can be applied to all SL- and ML-PNRs with an even number of phosphorus atoms in the width of the layer. The tight-binding model of phosphorene is given by the effective four-band Hamiltonian, considering one electron per lattice site. The tight-binding formula for SL- and ML- phosphorene materials is defined as follows [28]:

$$H = \sum_{i \neq j} t_{ij}^{\parallel} c_i^{\dagger} c_j + \sum_{i \neq j} t_{ij}^{\perp} c_i^{\dagger} c_j \qquad (1)$$

Where i and j run over the lattice sites, $t^{\parallel}$ ($t^{\perp}$) is the inlayer (interlayer) hopping parameter between the sites i and j, and $c_i^{\dagger}$ (c_j) is the creation (annihilation) operator of electrons at site i (j). The first term stands for the inlayer interactions between phosphorus atoms, and the second term describes the interactions between atoms belonging to different layers. We note that the Hamiltonian given by (Eq. 1) does not contain on-site terms, meaning that electrons have equivalent energies at all the sites.

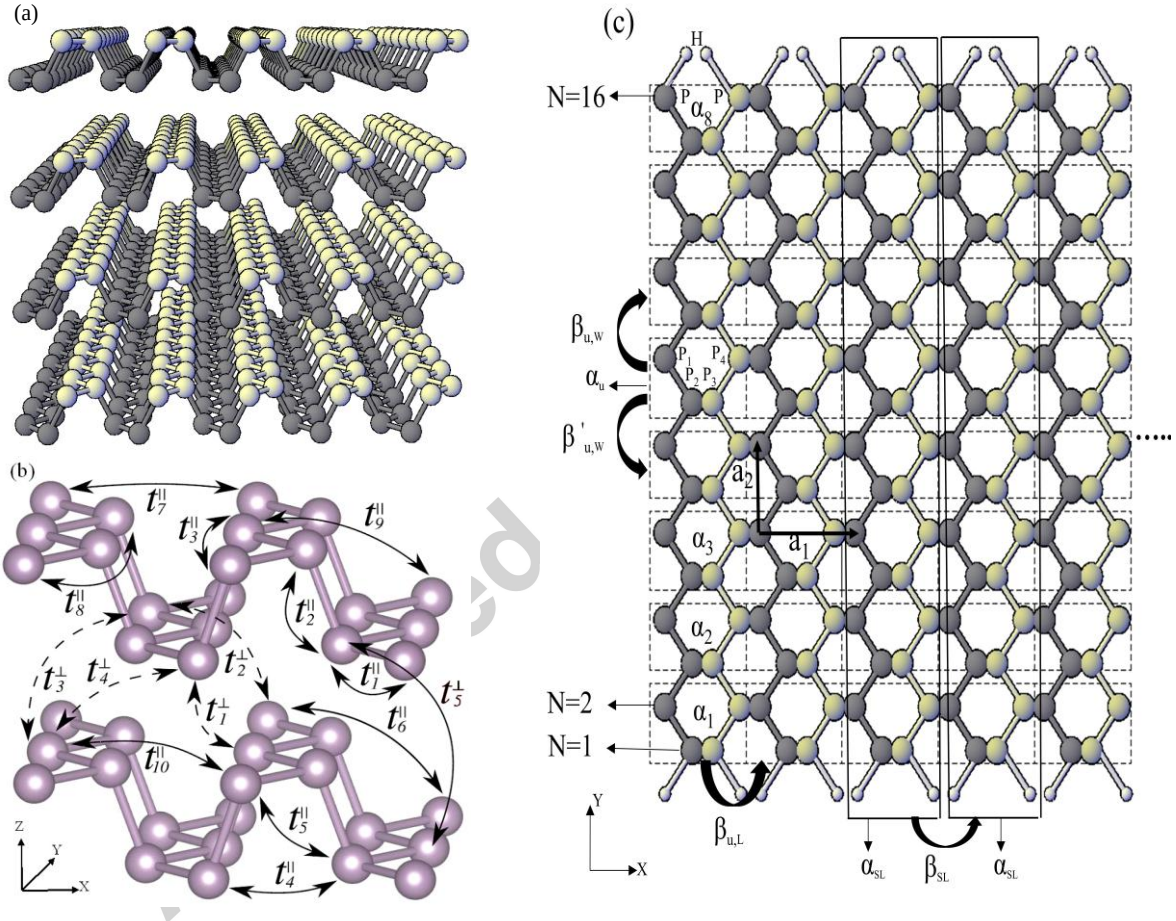

Fig. 1. (a) Front view of atomic structure of multilayer phosphorene. (b) Schematic representation of the hopping parameters for the tight-binding model applied to the multilayer black phosphorus. The corresponding values are given in Table I [28]. (c) Top view of ball-stick model of atomic structures for single layer, (SL) 16-A-PNR. The unit cells α_u's are marked by dashed squares. The edge dangling bonds are passivated by hydrogen atoms (in white).

First, we define a unit cell including four phosphorus atoms as shown in Fig. 1 (c). The 4-atom unit cell is distributed in the transverse direction (y-direction) to make a large unit cell which makes the width of the ribbon. Then, we distribute the new large unit cell along the transport direction (x-direction) in order to construct the full Hamiltonian matrix, H, of the A-PNR structure. The new tight-binding parameters for inlayer and interlayer interactions in phosphorene multilayer structures are introduced in Fig. 1 (b) and the values are given in Table I [28].

Using the phosphorene structure and the unit cells shown in Fig. 1 (c), we have the Hamiltonian matrix α_u for each individual unit cell as follows:

$$a_u = \begin{bmatrix} 0 & t^{\parallel}_1 & t^{\parallel}_5 & t^{\parallel}_6 \\ t^{\parallel}_1 & 0 & t^{\parallel}_2 & t^{\parallel}_5 \\ t^{\parallel}_5 & t^{\parallel}_2 & 0 & t^{\parallel}_1 \\ t^{\parallel}_6 & t^{\parallel}_5 & t^{\parallel}_1 & 0 \end{bmatrix} \quad (2)$$

$\beta_{u,W}$ is a matrix with the same size as α_u describes the interactions between each two neighbor small unit cells in the direction across the width of the PNR.

$$\beta_{u,W} = \begin{bmatrix} t^{\parallel}_3 & t^{\parallel}_1 & t^{\parallel}_5 & t^{\parallel}_9 \\ t^{\parallel}_8 & t^{\parallel}_3 & 0 & 0 \\ 0 & 0 & t^{\parallel}_3 & t^{\parallel}_8 \\ t^{\parallel}_9 & t^{\parallel}_5 & t^{\parallel}_1 & t^{\parallel}_3 \end{bmatrix} \quad (3)$$

$B_{u,W,F}$ describes the lateral interaction between two unit cell atoms like unit cells α_{u1} and α_{u3}.

$$\beta_{u,W,F} = \begin{bmatrix} 0 & t^{\parallel}_8 & 0 & 0 \\ 0 & 0 & 0 & 0 \\ 0 & 0 & 0 & 0 \\ 0 & 0 & t^{\parallel}_8 & 0 \end{bmatrix} \quad (4)$$

$\beta_{u,L}$ describes the interactions between each adjoining unit cell in the transport direction (x-direction). Other matrices are also defined in the same way.

$$\beta_{u,L} = \begin{bmatrix} t^{\parallel}_7 & 0 & 0 & 0 \\ t^{\parallel}_4 & t^{\parallel}_7 & 0 & 0 \\ t^{\parallel}_5 & t^{\parallel}_6 & t^{\parallel}_7 & 0 \\ t^{\parallel}_2 & t^{\parallel}_5 & t^{\parallel}_4 & t^{\parallel}_7 \end{bmatrix} \quad \beta_{u,L,F} = \begin{bmatrix} t^{\parallel}_{10} & 0 & 0 & 0 \\ 0 & t^{\parallel}_{10} & 0 & 0 \\ 0 & t^{\parallel}_9 & t^{\parallel}_{10} & 0 \\ 0 & t^{\parallel}_5 & t^{\parallel}_4 & t^{\parallel}_{10} \end{bmatrix} \quad \beta_{u,L,B} = \begin{bmatrix} t^{\parallel}_{10} & 0 & 0 & 0 \\ t^{\parallel}_4 & t^{\parallel}_{10} & 0 & 0 \\ t^{\parallel}_5 & t^{\parallel}_9 & t^{\parallel}_{10} & 0 \\ 0 & 0 & 0 & t^{\parallel}_{10} \end{bmatrix} \quad (5)$$

where F and B stand for front and back, respectively. Now, we can define a super unit cell which is one single column of each individual unit cell in the width of the ribbon (y-direction) with only one unit cell length in the transport direction called α_{SL} as shown in Fig. 1 (c). The same thing can be used for interaction matrix β_{SL}, which is another single-column matrix describing the connections between two super unit cells of α_{SL}. By using α_{SL}, we can work on the problem as a one-dimensional system.

$$\alpha_{SL} = \begin{bmatrix} \alpha_u & \beta_{u,W} & \beta_{u,W,F} & 0 & 0 \\ \beta^{+}_{u,W} & \alpha_u & \beta_{u,W} & \beta_{u,W,F} & 0 \\ \beta^{+}_{u,W,F} & \beta^{+}_{u,W} & \alpha_u & \beta_{u,W} & \ddots \\ 0 & \beta^{+}_{u,W,F} & \beta^{+}_{u,W} & \alpha_u & \ddots \\ 0 & 0 & \ddots & \ddots & \ddots \end{bmatrix}_{2N\times 2N} \quad \beta_{SL} = \begin{bmatrix} \beta_{u,L} & \beta_{u,L,F} & 0 & 0 & 0 \\ \beta_{u,L,B} & \beta_{u,L} & \beta_{u,L,F} & 0 & 0 \\ 0 & \beta_{u,L,B} & \beta_{u,L} & \beta_{u,L,F} & 0 \\ 0 & 0 & \beta_{u,L,B} & \beta_{u,L} & \ddots \\ 0 & 0 & 0 & \ddots & \ddots \end{bmatrix}_{2N\times 2N} \quad (6)$$

N is the number of phosphorus atoms in the width of the nanoribbon. Therefore, the total number of atoms inside the channel of the device equals 2N times the number of the unit cells in the transport direction named as N_T. Thus, the size of Hamiltonian is $(2N\times N_T)\times(2N\times N_T)$.

TABLE I. Inlayer ($t^{\parallel}$) and interlayer ($t^{\perp}$) hopping parameters for multilayer black phosphorus, d denotes the distances between the corresponding interacting lattice sites. The hopping parameters are schematically shown in Fig. 1b [28].

No.	Inlayer		No.	Inlayer		No.	Interlayer	
	$t^{\parallel}$ (eV)	$d_{\parallel}$(A°)		$t^{\parallel}$ (eV)	$d_{\parallel}$(A°)		$t^{\perp}$ (eV)	$d_{\perp}$(A°)
1	-1.486	2.22	6	0.186	4.23	1	0.524	3.60
2	3.729	2.24	7	-0.063	4.37	2	0.180	3.81
3	-0.252	3.31	8	0.101	5.18	3	-0.123	5.05
4	-0.071	3.34	9	-0.042	5.37	4	-0.168	5.08
5	0.019	3.47	10	0.073	5.49	5	0.005	5.44

$$H_{SL}=\begin{bmatrix}\alpha_{SL} & \beta_{SL} & 0 & 0\\ \beta_{SL}^{+} & \alpha_{SL} & \beta_{SL} & 0\\ 0 & \beta_{SL}^{+} & \alpha_{SL} & \ddots\\ 0 & 0 & \ddots & \ddots\end{bmatrix}_{(2N*N_T)*(2N*N_T)} \tag{7}$$

For multilayer PNR structures, the same method can be used to determine their Hamiltonian. Here we define the interaction matrices between adjacent layers by γ. When we have interactions between two layers, the size of the smallest matrices will be 8*8, because they are made up of two unit cells in two different layers. Here, γ_W and γ_L are defined in the same way as β_W and β_L, respectively, but with different sizes and coefficients due to the increased number of phosphorene layers. Based on the previous explanation, the matrices for multilayer PNR are obtained as follows:

$$\gamma_{u,W}=\begin{bmatrix}0 & t^{\perp}_{5} & 0 & 0\\ t^{\perp}_{5} & 0 & 0 & 0\\ t^{\perp}_{2} & t^{\perp}_{1} & 0 & t^{\perp}_{5}\\ t^{\perp}_{4} & t^{\perp}_{2} & t^{\perp}_{5} & 0\end{bmatrix}\quad \gamma_{u,W,F}=\begin{bmatrix}0 & t^{\perp}_{5} & 0 & 0\\ 0 & 0 & 0 & 0\\ t^{\perp}_{3} & t^{\perp}_{1} & 0 & 0\\ t^{\perp}_{4} & t^{\perp}_{3} & t^{\perp}_{5} & 0\end{bmatrix}\quad \gamma_{u,W,B}=\begin{bmatrix}0 & t^{\perp}_{5} & 0 & 0\\ t^{\perp}_{5} & 0 & 0 & 0\\ t^{\perp}_{3} & t^{\perp}_{1} & 0 & 0\\ 0 & t^{\perp}_{3} & 0 & 0\end{bmatrix} \tag{8}$$

$$\gamma_{W}=\begin{bmatrix}\gamma_{u,W} & \gamma_{u,W,F} & 0 & 0\\ \gamma_{u,W,B} & \gamma_{u,W} & \gamma_{u,W.F} & 0\\ 0 & \gamma_{u,W,B} & \gamma_{u,W} & \ddots\\ 0 & 0 & \ddots & \ddots\end{bmatrix}_{2N\times 2N}\quad \gamma_{u,\mathrm{L}}=\begin{bmatrix}0 & 0 & 0 & 0\\ 0 & 0 & 0 & 0\\ t^{\perp}_{2} & t^{\perp}_{3} & 0 & 0\\ t^{\perp}_{1} & t^{\perp}_{2} & 0 & 0\end{bmatrix}\quad \gamma_{u,\mathrm{L,F}}=\begin{bmatrix}0 & 0 & 0 & 0\\ 0 & 0 & 0 & 0\\ t^{\perp}_{3} & 0 & 0 & 0\\ t^{\perp}_{1} & t^{\perp}_{3} & 0 & 0\end{bmatrix}$$

$$\gamma_{u,\mathrm{L,B}}=\begin{bmatrix}0 & 0 & 0 & 0\\ 0 & 0 & 0 & 0\\ t^{\perp}_{3} & t^{\perp}_{4} & 0 & 0\\ 0 & t^{\perp}_{3} & 0 & 0\end{bmatrix}\quad \gamma_{L}=\begin{bmatrix}\gamma_{u,\mathrm{L}} & \gamma_{u,\mathrm{L},F} & 0 & 0\\ \gamma_{u,\mathrm{L},B} & \gamma_{u,\mathrm{L}} & \gamma_{u,\mathrm{L},F} & 0\\ 0 & \gamma_{u,\mathrm{L},B} & \gamma_{u,\mathrm{L}} & \ddots\\ 0 & 0 & \ddots & \ddots\end{bmatrix}_{2N\times 2N}$$

In the case of multilayer, different types of relative location of atoms in adjacent layers are known which are called AA-, AB-, and AC-stacking [27]. Finally, we can define α_{ML}, β_{ML}, and H_{ML} for AB-stacked multilayer phosphorene materials as follows [27]:

$$\alpha_{ML}=\begin{bmatrix}\alpha_{SL} & \gamma_{W} & 0 & 0\\ \gamma_{W}^{+} & \alpha_{SL} & \gamma_{W} & 0\\ 0 & \gamma_{W}^{+} & \alpha_{SL} & \ddots\\ 0 & 0 & \ddots & \ddots\end{bmatrix}\quad \beta_{ML}=\begin{bmatrix}\beta_{SL} & \gamma_{L} & 0 & 0\\ 0 & \beta_{SL} & \gamma_{L} & 0\\ 0 & 0 & \beta_{SL} & \ddots\\ 0 & 0 & \ddots & \ddots\end{bmatrix} \tag{9}$$

Using the time-independent Schrödinger equation and Bloch's theorem in periodic structures, the band structure of the SL- and ML-PNRs can be calculated using the following formulas SL and ML cases, respectively [31]:

$$E(k)=\alpha_{SL}+\beta_{SL}e^{ika}+\beta_{SL}^{+}e^{-ika} \tag{10-a}$$

$$E(k)=\alpha_{ML}+\beta_{ML}e^{ika}+\beta_{ML}^{+}e^{-ika} \tag{10-b}$$

where k is the momentum.

Formula (10) is used to plot the band structure of materials for the first Brillouin zone. The band gap can be easily calculated using the band structure of material by finding the minimum and maximum energies of conduction and valance bands respectively. We can also make the complete Hamiltonian of the multilayer structure using the Hamiltonian of each individual layer and the interaction matrices with its neighboring layers as follows:

$$H_{SL}=\begin{bmatrix}\alpha_{SL} & \beta_{SL} & 0 & 0\\ \beta_{SL}^{+} & \alpha_{SL} & \beta_{SL} & 0\\ 0 & \beta_{SL}^{+} & \alpha_{SL} & \ddots\\ 0 & 0 & \ddots & \ddots\end{bmatrix}\quad \gamma_{SL}=\begin{bmatrix}\gamma_{W} & \gamma_{L} & 0 & 0\\ \gamma_{L}^{+} & \gamma_{W} & \gamma_{L} & 0\\ 0 & \gamma_{L}^{+} & \gamma_{W} & \ddots\\ 0 & 0 & \ddots & \ddots\end{bmatrix}\quad H_{ML}=\begin{bmatrix}H_{SL} & \gamma_{SL} & 0 & 0\\ \gamma_{SL}^{+} & H_{SL} & \gamma_{SL} & 0\\ 0 & \gamma_{SL}^{+} & H_{SL} & \ddots\\ 0 & 0 & \ddots & \ddots\end{bmatrix} \tag{11}$$

Now, we have defined all the required matrices corresponding to the atomic structure of the channel, the source and the drain. Thus, we can find the retarded Green's function as follows [31]:

$$G(E) = [(\mathrm{E}+\mathrm{i}0^{+})I - H - U - \Sigma_S - \Sigma_D]^{-1} \quad (12)$$

where E is the energy, $\Sigma_{S/D}$ is the self-energy matrix of the source/drain, and I is the identity matrix. U is the diagonal matrix of potential calculated from solving the Poisson's equation in the device, and its diagonal elements are the potential of individual atoms inside the channel of the device. We numerically calculate the transmission and the electron density using the Green's function. Then, electron density is put into the Poisson's equation to find the potential in the device. The electron density and chemical potential are determined self consistently after several iterations. When the self-consistency between the quantum transport equation and Poisson's equation is achieved, the source-drain current density is computed by using the Landauer formula as follows [31]:

$$I_{ds} = \frac{2q}{h}\frac{1}{W}\int T(\mathrm{E})\left[f(\mathrm{E}-\mu_S) - f(\mathrm{E}-\mu_D)\right]dE \quad (13)$$

where W is the width of channel, f is the fermi function, and $\mu_{S/D}$, as the chemical potential at the source/drain contact, is defined with respect to the Fermi level of the source electrode. T(E) is the source-drain transmission calculated using the following formula:

$$\mathrm{T}(E) = Trace\left[\Gamma_S(E)G(E)\Gamma_D(E)G'(E)\right] \quad (14)$$

where $\Gamma_{S(D)}$ is the broadening quantity of each contact calculated numerically using the self-energy matrix of each one as follows:

$$\Gamma_{S(D)}(E) = \mathrm{i}\left[\Sigma_{S(D)} - \Sigma_{S(D)}^{+}\right] \quad (15)$$

3. Results and Discussion

The schematic structure of PNRFET is shown in Fig. 2, composed of n-type source and drain regions with an intrinsic channel region with a length that varies from 5nm to 15nm in this study. The lengths of source and drain regions are 7.1nm each to fulfill the ITRS 2028 node requirement, and no gate contact overlap/underlap for the device is considered. In order to satisfy the ITRS requirement, the 2nm thick gate oxide insulator HfO_2 with relative dielectric constant of ε_r = 25 is considered to improve the gate electrostatic control over the channel. The gate voltage, V_{gs} is applied as the boundary condition at the interface between the gate electrodes and the gate oxides. For the artificial boundaries, the Neumann boundary condition is used, where the electric field perpendicular to the boundary is assumed to be zero. As mentioned before, in the quantum transport model for nano-device analysis based on the tight-binding approach, the device structure is described by a Hamiltonian matrix, H. The electron density and chemical potential are determined self consistently after several iterations. Finally, I-V characteristics of the device under different biases are obtained. The simulations are performed at the room temperature, T=300 K. The simulation results are arranged in two parts as follows:

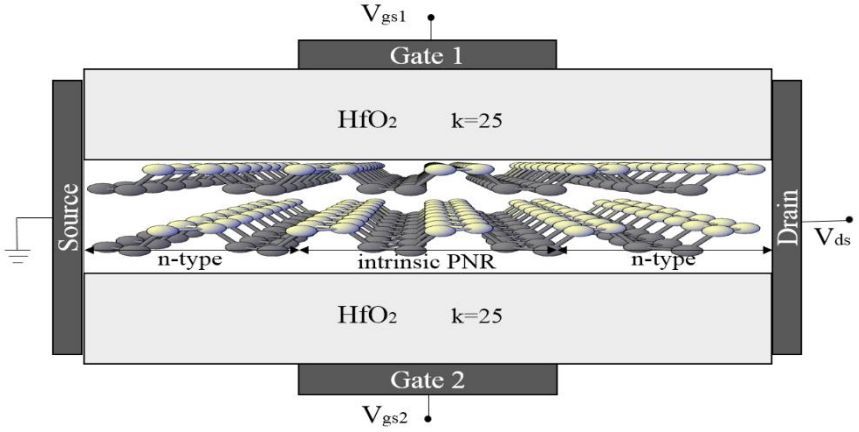

Fig. 2. The schematic structure of multilayer phosphorene FET, composed of n-type source and drain regions with an intrinsic channel region. The length of source and drain regions is 7.1nm each. A 2nm HfO_2 with dielectric constant of ε_r = 25 is used as the gate oxide insulator.

3.1 Electronic properties of phosphorene nanoribbon

Calculations of the band gap of different PNRs are performed based on the above matrix representation. Fig. 3 shows the band gap variation of A-PNRs versus the number of atoms in the width of the PNR. As shown, A-PNR is a semiconductor material, and its band gap decreases as the width of the nanoribbon increases due to the quantum confinement effect [15, 33, 34]. The band gap of the single layer PNR reaches a saturated value of 1.84 eV when the width of the ribbon increases significantly. The band gap values of single layer and multilayer A-PNRs calculated in this work are in close agreement with the previous reports which used first principle calculations and the tight-binding method [28]. When we increase the number of layers, the band gap decreases from the saturated value of 1.84eV to 1.14, 0.845, and 0.692 eV for 1L-, 2L-, 3L-, and 4L-PNR, respectively, where they are in close agreement with the previous report [28]. It confirms the accuracy of our TB method which is implemented in our simulation of the PNRFET.

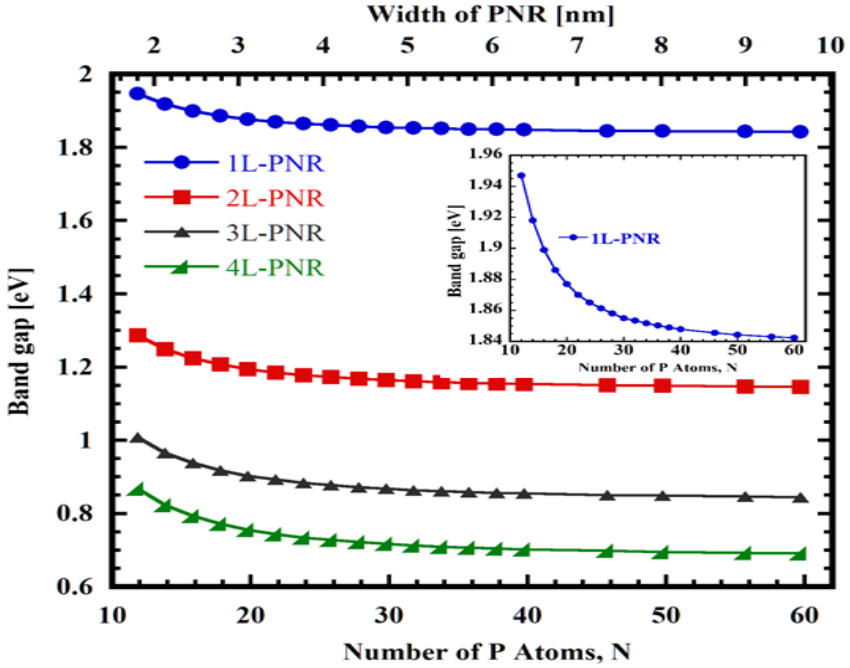

Fig. 3. Band gap variation of multilayer A-PNRs vs. the width and the number of phosphorus atoms across the width of PNR. Inside graph shows the band gap variation for single layer A-PNR versus the number of atoms across the width.

Fig. 4 shows the energy band structure of 1L-, 2L-, and 3L-PNRs with 16 phosphorus atoms in the widths of the A-PNRs. By increasing the number of PNR layers, the band gap of a multilayer PNR becomes smaller than that of the single layer counterpart.

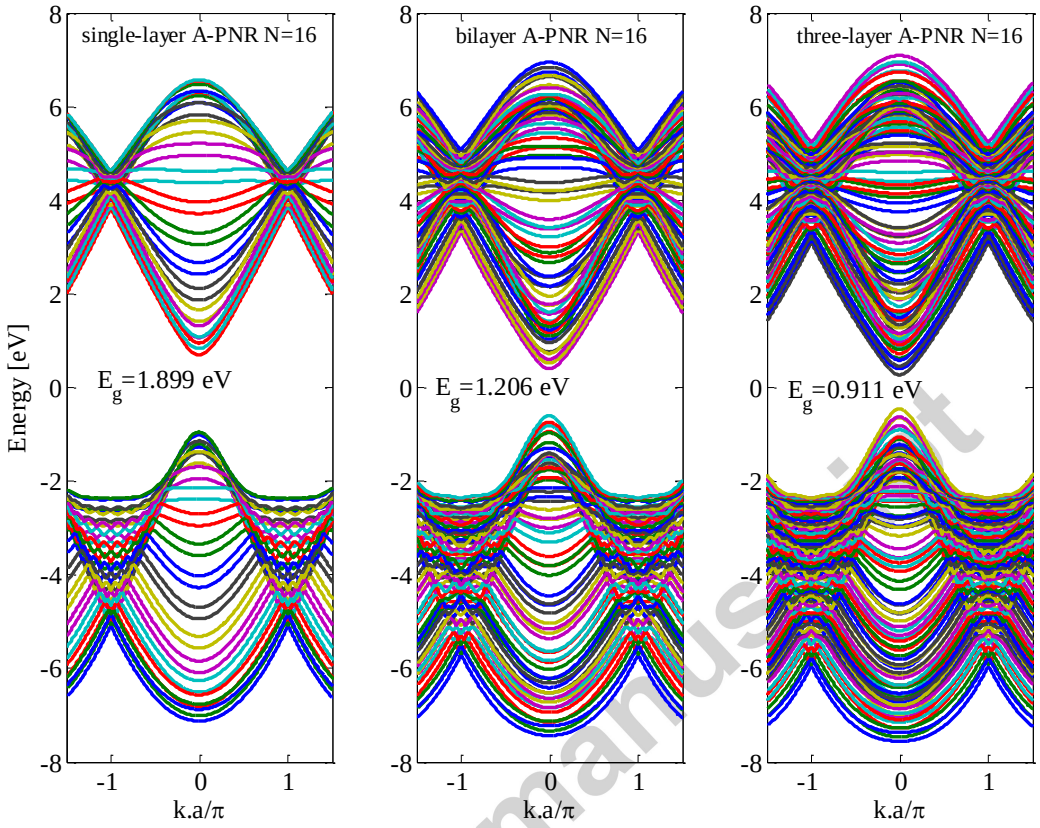

Fig. 4. Energy band diagrams of 1L-, 2L-, and 3L-PNR structures of 16 phosphorus atoms across the width of PNR.

3.2 Simulation results for Phosphorene FETs

In order to clearly show the difference between single-layer and multilayer phosphorene FETs, we define the current at the bias point of $V_{gs,OFF}=V_{dd}/2=0.25$ V as the off-current, and the current at the bias point of $V_{gs,ON}=V_{gs,OFF}+V_{dd}=0.75$ V for $V_{dd}=0.5$ V as the on-current [35]. In this case, we suppose that the gate contacts have the same work function as that of the channel material. Alternatively, we could consider 0.25 V as the difference between the work functions of gate contacts and the channel material to be used as a device adjusting parameter to investigate the OFF current at $V_{gs,OFF}=0$ and $V_{gs,ON}=0.5$ V.

Logarithmic and linear scales of I_{ds} versus V_{gs} for SL- and ML-A-PNRFETs of N=16 and channel lengths of $L_{ch}=5$ and 10nm are shown in Fig. 5. As stated before, increasing the number of PNR layers reduces the band gap of material. Having a smaller band gap, the turn on voltage for the PNRFET reduces and the on-current increases. At the same time, the off-current also increases due to a higher probability of tunneling in low band gap devices. I_{ds} versus V_{ds} for ML-A-PNRFETs of $L_{ch}=5$nm with N=12, 14, and 16 are presented in Fig 6. It can be seen that the I_{ds} increases with increasing the number of layers due to increasing the number of transmission channels in multilayer structures. For example, for $V_{ds}=V_{gs}=0.5$ V and N=16, the current is 0.627, 292.6, and 1161 μA/μm for 1L-, 2L-, and 3L-PNRFETs, respectively. Also, ss shown for all structures, increasing the number of atoms across the width of A-PNR leads to an increase in I_{ds} due to the decrease of the band gap.

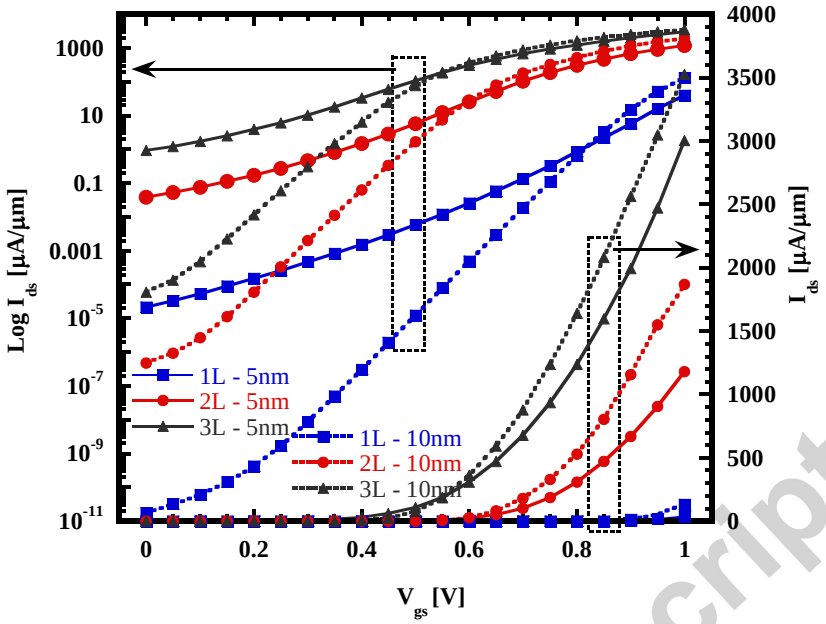

Fig. 5. The current I_{ds} vs. V_{gs} of multilayer A-PNRFETs of N=16 and L_{ch}=5 and 10nm.

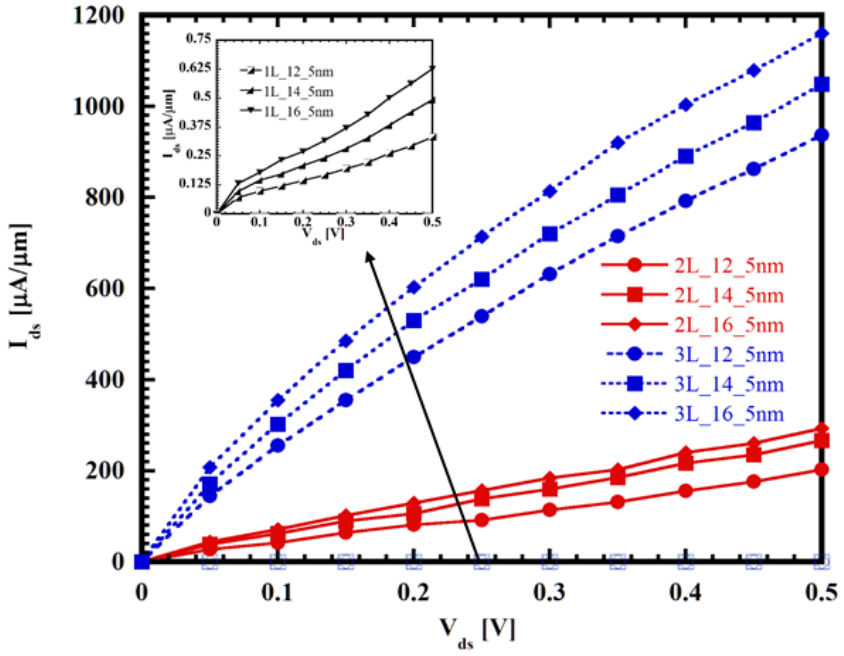

Fig. 6. The current I_{ds} vs. V_{ds} for multilayer A-PNRFETs of different Ns at $V_{gs}=V_{on}$. N is the number of phosphorus atoms in the width of the PNR. Due to the large difference between the scales of currents in SL- and ML-PNR, the I_{ds} vs. V_{ds} curves of the single layer A-PNRFET of N=12, 14, and 16 are displayed inside.

In Fig. 7, the current-voltage characteristics of 2L- and 3L-PNRFETs at higher drain-source voltages are simulated to show the saturation behavior of the device for the purpose of analyzing its transconductance coefficient. We cannot see the saturation behavior in Fig. 6 due to the channel length of 5nm. In this case, the device seriously suffers from short channel effects; however, as shown in Figure 7, devices with channel lengths of at least 7.5nm have good saturation behaviors.

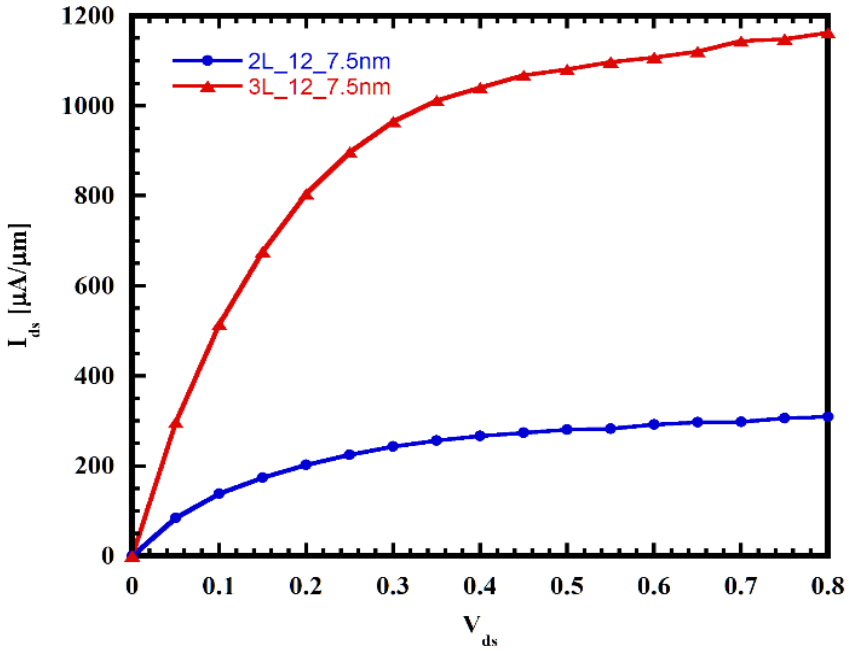

Fig. 7. The current I_{ds} vs. V_{ds} for 2L- and 3L-PNRFETs with N=12 and channel length of 7.5nm at $V_{gs}=V_{on}$.

The energy band structure of SL- and ML-PNRFETs are presented in Fig. 8. Fig. 8 also demonstrates the potential profiles of ML-PNRFETs of different channel lengths in both off- and on-states. The band gaps of material are 1.947, 1.287, and 1.008 eV for 1L-, 2L-, and 3L 12-APNRs which are well-suited in Fig. 8.

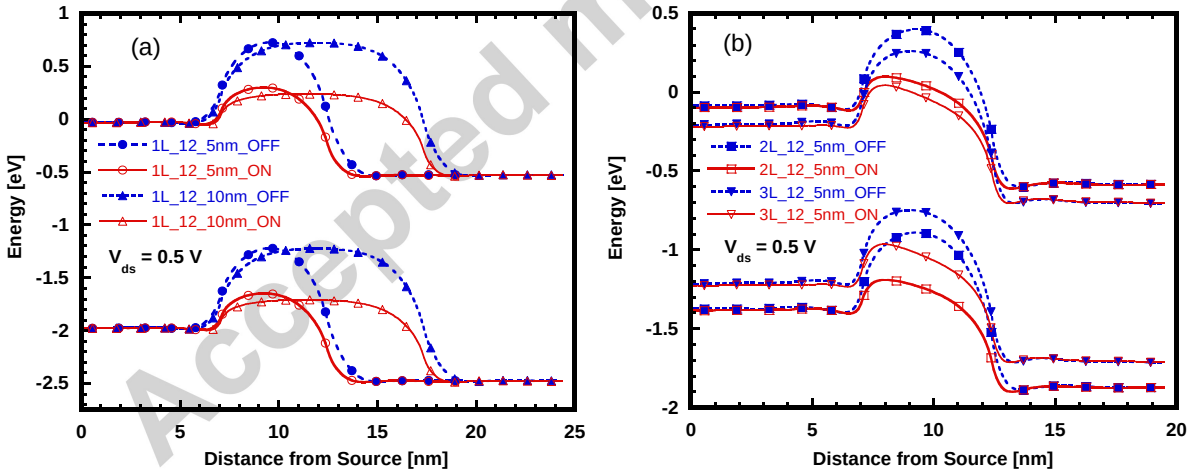

Fig. 8. (a) The energy band structure of 1L-PNRFET of L_{ch}=5 and 10nm in both OFF and ON states. (b) The energy band structure of 2L- and 3L-PNRFETs of L_{ch}=5 in both OFF and ON states.

It can be observed from Fig. 8, that in longer channel devices, the gate can control the ON current more effectively, where it is in correlation with the results shown in Fig. 7. On the other hand, in A-PNRFETs, as the number of layers rises, the band gap decreases and causes the current to increase, where such a behavior confirms the results presented in Figs. 5, 6 and 7.

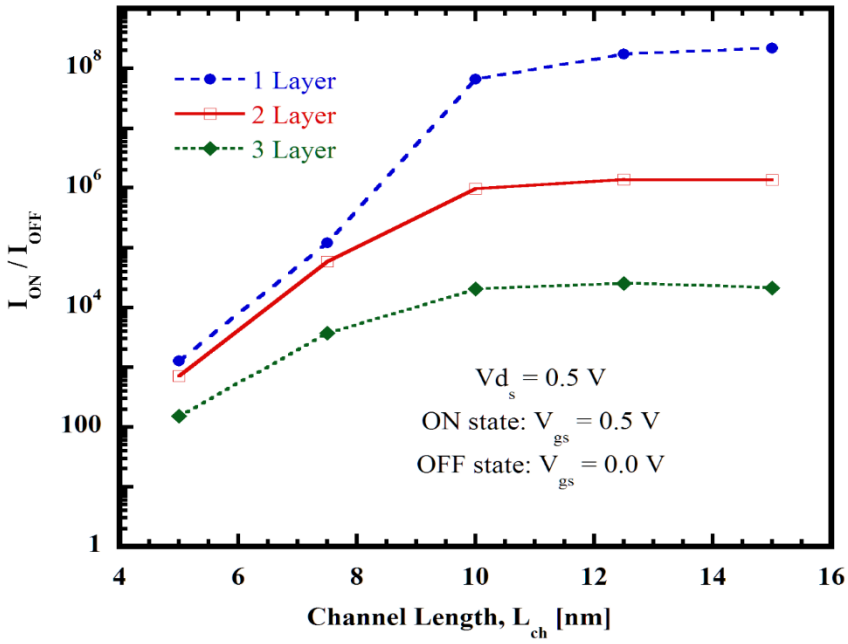

Fig. 9. The current ratio (I_{on}/I_{off}) versus channel length for ML-PNRFETs. The number of phosphorus atoms in the edge of material is considered to be N=12.

The role of I_{ON}/I_{OFF} of FETs in digital applications is essential, thus it is worth to be investigated. Fig. 9 shows the current ratio, I_{ON}/I_{OFF}, as the channel length scales down in ML-PNRFETs of N=12. We observe that for all cases, both on- and off-currents increase by decreasing the channel length. Off-current is the main factor of low-power transistor design which is increased by scaling down the channel length. The ON and OFF current ratios for L_{ch}=5nm in all 1L-, 2L-, and 3L-PNRFETs are approximately equal to 1000, however, for L_{ch}=15nm they are almost saturated and equal to 216.7×10^6, 1.350×10^6, and 21.2×10^3, respectively. The current ratio for single layer increases from 1277 for L_{ch}=5nm to 216.7×10^6 for L_{ch}=15nm. The I_{ON}/I_{OFF} in 1L-PNRFET is higher in comparison with those values in 2L- and 3L-PNRFETs due to very small off-current in the 1L-PNRFET which in turn resulted from its larger band gap.

4. Conclusion

Using the recently modified TB parameters of phosphorene, we have presented a matrix representation for multilayer PNRs. The matrices are useful for simulation of electrical and mechanical properties of armchair and zigzag ML phosphorene structures and the characteristics of phosphorene MOSFETs using the quantum transport approach. By this representation, we have investigated the performance of doped contact ML-A-PNRFETs through implementing quantum transport method based on non-equilibrium Green's function formalism. We showed that increasing the number of PNR layers reduces the band gap of material and the turn on voltage of PNRFET, but increases the on-current of device. Simultaneously, the off-current also increases due to a higher probability of tunneling in low band gap devices. In addition, increasing the number of atoms across the width of PNR leads to an increase in the I_{ds} due to the decrease of the band gap. Moreover, both on- and off-currents increase by decreasing the channel length in multilayer PNRFETs. Finally, it can be concluded that the ML-A-PNRFET is preferable over SL-A-PNRFET for some aspects of electrical behavior such as ON current and I_{ON}/I_{OFF}.

ACKNOWLEDGMENT

We would like to thank the Information Technology Department and Center for Computational Sciences at the University of Kentucky for computing time on the Lipscomb High Performance Computing Cluster and for accessing to other supercomputing resources.

References:

[1] R.-H. Kim, M.-H. Bae, D.G. Kim, H. Cheng, B.H. Kim, D.-H. Kim, M. Li, J. Wu, F. Du, H.-S. Kim, Stretchable, transparent graphene interconnects for arrays of microscale inorganic light emitting diodes on rubber substrates, Nano letters, 11 (2011) 3881-3886.
[2] M. Pumera, Graphene-based nanomaterials for energy storage, Energy & Environmental Science, 4 (2011) 668-674.
[3] P. Avouris, Graphene: electronic and photonic properties and devices, Nano letters, 10 (2010) 4285-4294.
[4] H. Sarvari, R. Ghayour, E. Dastjerdy, Frequency analysis of graphene nanoribbon FET by Non-Equilibrium Green's Function in mode space, Physica E: Low-dimensional Systems and Nanostructures, 43 (2011) 1509-1513.
[5] X. Chen, D. Akinwande, K.-J. Lee, G.F. Close, S. Yasuda, B.C. Paul, S. Fujita, J. Kong, H.-S.P. Wong, Fully integrated graphene and carbon nanotube interconnects for gigahertz high-speed CMOS electronics, IEEE Transactions on Electron Devices, 57 (2010) 3137-3143.
[6] A. Castellanos-Gomez, L. Vicarelli, E. Prada, J.O. Island, K. Narasimha-Acharya, S.I. Blanter, D.J. Groenendijk, M. Buscema, G.A. Steele, J. Alvarez, Isolation and characterization of few-layer black phosphorus, 2D Materials, 1 (2014) 025001.
[7] L. Li, Y. Yu, G.J. Ye, Q. Ge, X. Ou, H. Wu, D. Feng, X.H. Chen, Y. Zhang, Black phosphorus field-effect transistors, Nature nanotechnology, 9 (2014) 372-377.
[8] V. Tran, L. Yang, Scaling laws for the band gap and optical response of phosphorene nanoribbons, Physical Review B, 89 (2014) 245407.
[9] F. Xia, H. Wang, Y. Jia, Rediscovering black phosphorus: A unique anisotropic 2D material for optoelectronics and electronics, arXiv preprint arXiv:1402.0270, (2014).
[10] V.V. Kulish, O.I. Malyi, C. Persson, P. Wu, Adsorption of metal adatoms on single-layer phosphorene, Physical Chemistry Chemical Physics, 17 (2015) 992-1000.
[11] J. Zhang, H. Liu, L. Cheng, J. Wei, J. Liang, D. Fan, J. Shi, X. Tang, Q. Zhang, Phosphorene nanoribbon as a promising candidate for thermoelectric applications, Scientific reports, 4 (2014).
[12] F. Schwierz, Graphene transistors, Nature nanotechnology, 5 (2010) 487-496.
[13] P. Ruffieux, S. Wang, B. Yang, C. Sanchez, J. Liu, T. Dienel, L. Talirz, P. Shinde, C.A. Pignedoli, D. Passerone, On-surface synthesis of graphene nanoribbons with zigzag edge topology, arXiv preprint arXiv:1511.05037, (2015).
[14] Y.-W. Son, M.L. Cohen, S.G. Louie, Energy gaps in graphene nanoribbons, Physical review letters, 97 (2006) 216803.
[15] L. Yang, C.-H. Park, Y.-W. Son, M.L. Cohen, S.G. Louie, Quasiparticle energies and band gaps in graphene nanoribbons, Physical Review Letters, 99 (2007) 186801.
[16] H. Sarvari, Z. Chen, P. Shenavar, R. Ghayour, Investigation and Analysis of Single Layer Phosphorene Properties Based on Tight-Binding and Green's Function, in: The 24th Iranian Conference on Electrical Engineering (ICEE 2016), Shiraz, Iran, IEEE Xplore, 2016.
[17] E.T. Sisakht, M.H. Zare, F. Fazileh, Scaling laws of band gaps of phosphorene nanoribbons: A tight-binding calculation, Physical Review B, 91 (2015) 085409.
[18] Q. Wu, L. Shen, M. Yang, Y. Cai, Z. Huang, Y.P. Feng, Electronic and transport properties of phosphorene nanoribbons, Physical Review B, 92 (2015) 035436.
[19] J. Chang, C. Hobbs, Theoretical study of phosphorene tunneling field effect transistors, Applied Physics Letters, 106 (2015) 083509.

[20] H. Liu, A.T. Neal, Z. Zhu, Z. Luo, X. Xu, D. Tománek, P.D. Ye, Phosphorene: an unexplored 2D semiconductor with a high hole mobility, ACS nano, 8 (2014) 4033-4041.
[21] K.-T. Lam, Z. Dong, J. Guo, Performance limits projection of black phosphorous field-effect transistors, Electron Device Letters, IEEE, 35 (2014) 963-965.
[22] R. Wan, X. Cao, J. Guo, Simulation of phosphorene Schottky-barrier transistors, Applied Physics Letters, 105 (2014) 163511.
[23] X. Cao, J. Guo, Simulation of Phosphorene Field-Effect Transistor at the Scaling Limit, Electron Devices, IEEE Transactions on, 62 (2015) 659-665.
[24] S.P. Koenig, R.A. Doganov, H. Schmidt, A.C. Neto, B. Oezyilmaz, Electric field effect in ultrathin black phosphorus, Applied Physics Letters, 104 (2014) 103106.
[25] M.V. Kamalakar, B. Madhushankar, A. Dankert, S.P. Dash, Nanolayer Black-Phosphorous Field Effect Devices with Ferromagnetic Tunnel Contacts, arXiv preprint arXiv:1406.4476, (2014).
[26] S. Das, W. Zhang, M. Demarteau, A. Hoffmann, M. Dubey, A. Roelofs, Tunable transport gap in phosphorene, Nano letters, 14 (2014) 5733-5739.
[27] A. Mukhopadhyay, L. Banerjee, A. Sengupta, H. Rahaman, Effect of stacking order on device performance of bilayer black phosphorene-field-effect transistor, Journal of Applied Physics, 118 (2015) 224501.
[28] A. Rudenko, S. Yuan, M. Katsnelson, Toward a realistic description of multilayer black phosphorus: From G W approximation to large-scale tight-binding simulations, Physical Review B, 92 (2015) 085419.
[29] R. Saito, G. Dresselhaus, M.S. Dresselhaus, Physical properties of carbon nanotubes, World scientific, 1998.
[30] A.N. Rudenko, M.I. Katsnelson, Quasiparticle band structure and tight-binding model for single-and bilayer black phosphorus, Physical Review B, 89 (2014) 201408.
[31] S.D.Q. Transport, Atom to Transistor, edited by S. Datta, in, Cambridge University Press, 2005.
[32] E. Dastjerdy, R. Ghayour, H. Sarvari, 3D quantum mechanical simulation of square nanowire MOSFETs by using NEGF method, Central European Journal of Physics, 9 (2011) 472-481.
[33] X. Zhao, C. Wei, L. Yang, M. Chou, Quantum confinement and electronic properties of silicon nanowires, Physical review letters, 92 (2004) 236805.
[34] C.-H. Park, S.G. Louie, Energy gaps and stark effect in boron nitride nanoribbons, Nano letters, 8 (2008) 2200-2203.
[35] J. Guo, M. Lundstrom, Device simulation of SWNT-FETs, in: Carbon nanotube electronics, Springer, 2009, pp. 107-131.

Graphical Abstract

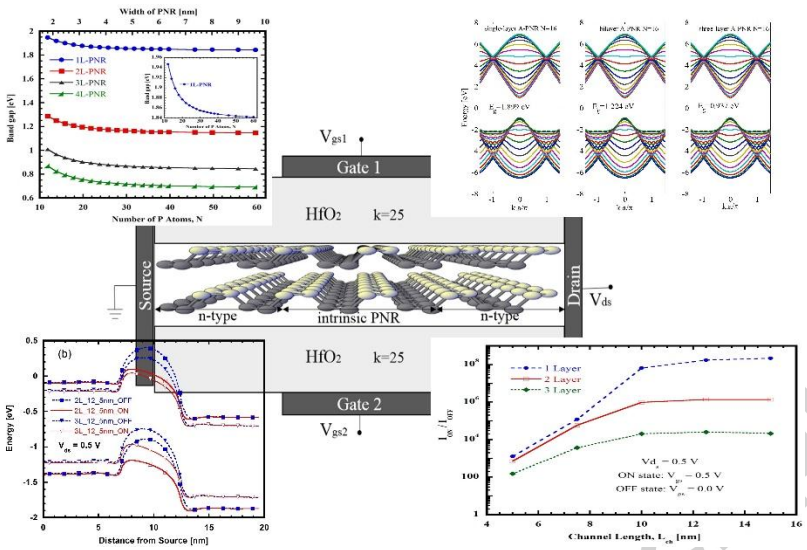

Highlights:

- We have used the tight-binding method to implement a matrix representation for single-layer (SL) and multilayer (ML) structures of armchair phosphorene nanoribbon (A-PNR).
- We have investigated the doped contact ML-A-PNR FETs using NEGF formalism.
- Increasing the number of A-PNR layers reduces the band gap of material and the turn on voltage of PNRFET, but increases the on-current of device.
- Increasing the number of atoms across the width of A-PNR leads to an increase in the I_{ds}.
- Both on- and off-currents increase by decreasing the channel length in ML-A-PNRFETs.